


Stealth Majorana zero mode in a trilayer heterostructure MnTe/Bi₂Te₃/Fe(Te, Se)Rui Song^{1,2} and Ning Hao^{2,*}¹*Science and Technology on Surface Physics and Chemistry Laboratory, Mianyang, Sichuan 621908, China*²*Anhui Key Laboratory of Condensed Matter Physics at Extreme Conditions, High Magnetic Field Laboratory, HFIPS, Chinese Academy of Sciences, Hefei, Anhui 230031, China* (Received 6 March 2023; revised 16 July 2023; accepted 31 August 2023; published 26 September 2023)

A recent experiment reported the presence of robust zero-energy states with peculiar properties in a trilayer heterostructure MnTe/Bi₂Te₃/Fe(Te, Se). In this study, we provide a comprehensive understanding of the magnetic and electronic properties of this heterostructure. We propose that magnetic Mn-Bi antisite defects are formed in the topmost sublayer of Bi₂Te₃ and remain hidden beneath the MnTe layer. Moreover, we reveal that these defects can give rise to two types of quasiparticles. First, the defect itself generates a Yu-Shiba-Rusinov state, and second, a pair of Majorana zero modes emerge from the superconducting phase domain wall induced by the defect. These two types of quasiparticles exhibit contrasting responses to magnetic fields, temperature, and other factors. The coexistence and mutual cooperation of both types of quasiparticles can account for the experimental observations. Furthermore, we propose a simpler heterostructure that possesses advantages in generating and finely modulating Majorana zero modes.

DOI: [10.1103/PhysRevB.108.L100509](https://doi.org/10.1103/PhysRevB.108.L100509)

Since the discovery of high-temperature superconductivity in FeSe/SrTiO₃ [1], there has been significant interest in exploring new interfacial physical phenomena in heterostructures involving Fe(Te,Se). These phenomena include spin density waves, interfacial phonon modes, topological physics, gating effects, and the competition between superconductivity and magnetism, etc. [2–9]. The superconductor-ferromagnetic hybrids have quickly become an excellent platform for exploring exotic superconducting states [10–29]. Recently, an unexpected robust zero-energy state was experimentally observed in a trilayer heterostructure MnTe/Bi₂Te₃/Fe(Te, Se) [30]. This state exhibits intriguing properties, such as invisibility in surface topography but visibility in zero-bias dI/dV maps, robustness against external magnetic fields, and unusual temperature evolution. The zero energy state can appear in both topological superconductors and topologically trivial superconductors with odd frequency. Both Bi₂Te₃ and Fe(Te,Se) are well-known topological materials, making it natural to associate the robustness of the zero-energy state with the system's nontrivial topology. However, the complexity of the trilayer heterostructure hampers a clear understanding of this connection. Consequently, the following urgent questions arise: Is the robust zero-energy state a Majorana zero mode (MZM)? How is it generated? How can one comprehend its peculiar properties? Addressing these questions could establish the trilayer heterostructure as a new platform for studying MZM physics or provide insights for constructing more practical systems to realize MZMs.

In this study, we comprehensively address the aforementioned issues by investigating the magnetic and electronic properties of trilayer heterostructures using density functional

theory (DFT) calculations. To understand the underlying physics of the zero-energy state, we develop a simplified theoretical model. Our DFT calculations suggest that a single unit cell (1-UC) of MnTe is likely to generate weak antiferromagnetic (AFM) fluctuations instead of long-range AFM order. The resulting band structures are consistent with experimental results obtained from quasiparticle interference (QPI) measurements. We propose the existence of at least two different types of point defects in the trilayer heterostructure. One type originates from vacancies of Te atoms on the top surface of the 1-UC MnTe/Bi₂Te₃/Fe(Te, Se) system. The other type is the Mn-Bi antisite defect, where a Mn atom substitutes a Bi atom in the top layer of Bi₂Te₃. The Mn-Bi antisite defect introduces a magnetic moment that couples with the surface electrons of Bi₂Te₃ in a ferromagnetic manner. This defect not only induces a trivial Yu-Shiba-Rusinov (YSR) state but also drives a local quantum phase transition (QPT) in the surface superconductivity of Bi₂Te₃ facilitated by the proximity effect from Fe(Te,Se). Specifically, the superconducting order parameter of Bi₂Te₃ near the defect undergoes a sign-change beyond the QPT. Consequently, a degenerate pair of Majorana zero modes (MZMs), protected by an emergent mirror symmetry, emerges and is trapped by the phase domain wall near the Mn-Bi antisite defect. The YSR state and MZMs exhibit distinct responses to external magnetic fields, temperature, and other factors. The coexistence and mutual cooperation of these two types of quasiparticles explain the experimentally observed properties of the quasiparticles within the superconducting gap that were previously perplexing. In the case of the trilayer heterostructure with 2-UC MnTe, our findings indicate a violation of the aforementioned picture, yielding only trivial results. Furthermore, we predict unexplored properties of the zero-energy state and propose simpler platforms to generate and modulate MZMs.

*haon@hmfl.ac.cn

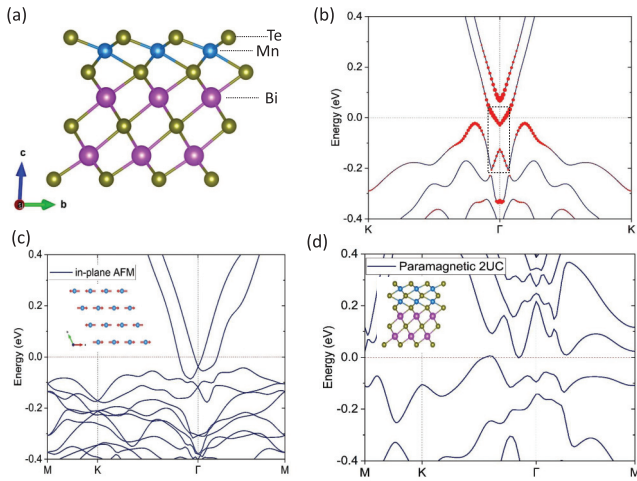


FIG. 1. (a) The heterostructure of MnTe/Be₂Te₃. (b) The band structure of heterostructure without long-range magnetic order in MnTe. The sizes of the red dots label the weight from the topmost sublayer of Be₂Te₃. The bands in the rectangle regime are captured by Eq. (2). (c) The band structure of heterostructure with in-plane AFM long-range order in MnTe. Inset gives the pattern of AFM order. (d) The band structure of heterostructure involving 2-UC MnTe in the absence of any long-range magnetic order. Inset gives the configuration of the heterostructure.

As confirmed by the experiment, the 1-UC MnTe shares the same crystal lattice constant as 1-UC Bi₂Te₃. In DFT calculations, we consider 1-UC Bi₂Te₃ as the substrate and neglect the influence of the bare Fe(Te,Se) substrate. The Fe(Te,Se) substrate only weakly affects the band structures of Bi₂Te₃, except for providing proximity-induced superconductivity [31,32]. We allow the MnTe layer to relax freely until it satisfies the force and energy criteria. The final structure is depicted in Fig. 1(a). The Te-Mn-Te sandwich structure is the same as that in the α -MnTe crystal [33,34]. We consider various magnetic orders for 1-UC MnTe, using the bulk α -MnTe's magnetic order as a reference. Our DFT results are consistent with the calculations in Ref. [30]. Additionally, we calculate the band structures of 1-UC MnTe/Bi₂Te₃ by assuming different long-range antiferromagnetic (AFM) or ferromagnetic (FM) orders (see the SM [35] for details). Fig. 1(c) demonstrates that the bands crossing the Fermi level around the Γ point split into a Rashba type, which is inconsistent with the parabolic type extracted by QPI measurements [30]. Thus, we propose that only weak AFM fluctuations exist in 1-UC MnTe, even though the DFT predicts that 1-UC MnTe with AFM-I order has the lowest energy. We argue that such discrepancies are not uncommon in low-dimensional systems. For instance, DFT predicts a checkerboard AFM order in monolayer FeSe/SrTiO₃ [43–46], but no experiment has observed such an order [47–52]. The observation of gapless Dirac-cone-like surface states in MnBi₂Te₄ also suggests the absence of long-range magnetic order in the topmost MnTe layer [53–56]. Our calculations also reveal a small magnetic anisotropy in 1-UC MnTe, further indicating the lack of long-range AFM order according to the Mermin-Wagner theorem [57]. Moreover, the experiment has observed an enhancement of superconductivity in the 1-UC MnTe trilayer

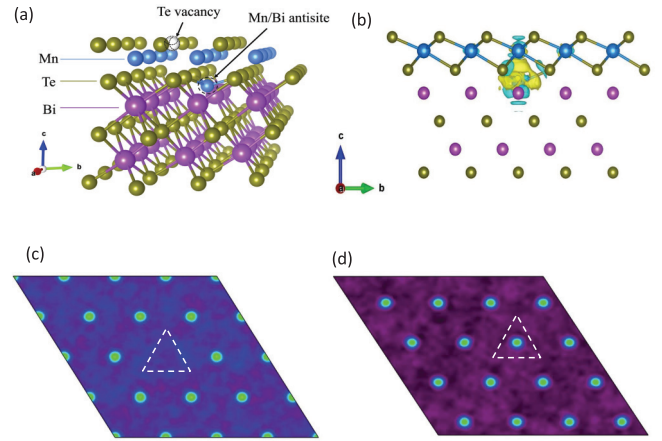


FIG. 2. (a) Two types of defects are schematically shown in the heterostructure. One is Te vacancy in the topmost sublayer of MnTe and another is Mn-Bi antisite in the topmost sublayer of Be₂Te₃. (b) The differential charge density distribution around the Mn-Bi antisite defect. [(c),(d)] The simulated STM images on topmost surface of the heterostructure including a Te vacancy in (c) and a Mn-Bi antisite defect in (d).

heterostructure. We propose that this enhancement arises from the effect of AFM fluctuations in 1-UC MnTe, as predicted by the theory of spin-fluctuation-mediated superconductivity. We will not delve further into the discussion of superconductivity enhancement here but will address it elsewhere. When the long-range AFM order is absent, the calculated band structure of 1-UC MnTe/Bi₂Te₃, as shown in Fig. 1(b), exhibits a simple parabolic-type band crossing the Fermi level, consistent with the results from QPI measurements [30]. Therefore, we conclude that the first effect of 1-UC MnTe in the trilayer structure is to introduce AFM fluctuations that enhance superconductivity, while the second effect is to shift the Fermi level through charge doping. Figure 1(d) demonstrates that only trivial band structure remains in the case of 2-UC MnTe, which we will not discuss further.

Remarkably, Mn-Bi and Bi-Te antisite defects of two types were experimentally observed in MnBi₂Te₄ [58]. It is reasonable to assume that similar antisite defects could exist at the interface between 1-UC MnTe and 1-UC Bi₂Te₃ in such a heterostructure. Specifically, the heterostructure is fabricated using the molecular beam epitaxy (MBE) method. Figure 2(a) illustrates the structures of two typical defects: a Te vacancy defect on the topmost sublayer of 1-UC MnTe and a Mn-Bi antisite defect where a Mn atom substitutes a Bi atom on the topmost sublayer of 1-UC Bi₂Te₃. Figure 2(b) displays the calculated distribution of differential charge density around the Mn-Bi antisite defect. It is evident that the charge transfer mainly occurs between the bottommost sublayer of 1-UC MnTe and the topmost layer of 1-UC Bi₂Te₃. Consequently, the charge density distribution is barely affected on the topmost surface of the heterostructure, making it difficult to detect and determine the positions of the Mn-Bi antisite defects through scanning tunneling microscopy (STM) topographic images. Figures 2(c) and 2(d) present the DFT simulated STM image, which reveals only the Te-vacancy defect. If the observed zero-energy states are closely related

to the Mn-Bi antisite defects, their random distribution can now be easily understood. Our calculations also indicate that the Mn-Bi antisite defect spontaneously induces a local magnetic moment of $4.8 \mu_B$ due to the magnetism of the Mn atom. In the following, we will demonstrate that the magnetic Mn-Bi antisite defects play a crucial role in generating the observed zero-energy states, which are indeed Majorana zero modes (MZMs). As the Mn-Bi antisite defects in the inner layer of the trilayer heterostructure cannot be detected by the charge distribution of the outer layer, but rather by the defect-bound superconducting quasiparticle tunnel spectrum, we refer to these zero-energy states as stealth MZMs. Hence, we conclude that the third effect of 1-UC MnTe in the trilayer structure is to introduce magnetic Mn-Bi antisite defects in the topmost sublayer of 1-UC Bi₂Te₃ in the trilayer heterostructure.

With the information presented above, we can construct an effective model to address how the robust zero-energy state is generated. The effective Hamiltonian is expressed as follows:

$$H_{\text{tot}} = H_{\text{sur}} + H_d + H_{\Delta}. \quad (1)$$

Here,

$$H_{\text{sur}} = v_F(k_x \sigma_y - k_y \sigma_x) - (\mu - Ak^2) + (\Lambda_0 - Bk^2)\sigma_z \kappa_z, \quad (2)$$

$$H_d = \int d\mathbf{r} J(\mathbf{r}) \mathbf{S}_{\text{def}} \cdot \boldsymbol{\sigma}, \quad H_{\Delta} = \Delta(\mathbf{r}) \tau_x. \quad (3)$$

Here, H_{sur} is the low-energy effective Hamiltonian to describe the surface bands of 1-UC MnTe/Bi₂Te₃ thin film [59], as indicated by the red dashed rectangle in Fig. 1(b). Note that we neglect the effect of structural inversion asymmetry because the Rashba-like splitting induced by such an effect is inconsistent with QPI measurements [30]. H_d describes the coupling between the magnetic Mn-Bi antisite defect and the surface electrons. H_{Δ} represents the proximity-induced superconducting pairing term from Fe(Te,Se). v_F is the Fermi velocity, μ is the chemical potential, Λ_0 measures the gap of the Dirac cone opened by finite-thickness effects, and A and B are coefficients of the second-order terms. $J(\mathbf{r}) = J\delta(\mathbf{r})$ describes the ferromagnetic coupling with a constant J . \mathbf{S}_{def} is the moment of the defect, having only a z component. $\Delta(\mathbf{r})$ is the superconducting order parameter induced by the proximity effect. Note that $\Delta(\mathbf{r})$ is constant without the defect. σ , κ , and τ represent the Pauli matrices that span the spin, pseudo-valley, and particle-hole subspaces, respectively. H_{tot} can be numerically solved in the lattice case [60] (see the SM [35] for details). The influence of the magnetic defect can be understood as follows: as $J(\mathbf{r} = 0)$ increases from zero, the impurity site's $\Delta(\mathbf{r} = 0)$ is suppressed and reaches zero at a critical J_c . Beyond J_c , $\Delta(\mathbf{r} = 0)$ changes sign [61–67]. This implies the existence of a QPT at the critical J_c . Simultaneously, the hole-type and electron-type branches of YSR states [68–70] undergo a process of approaching, crossing, and separating as $J(\mathbf{r} = 0)$ increases from zero. The critical physical quantity J_c can be estimated through calculations, and we find $J_c \sim 4.2v_F k_F$ with $v_F k_F \sim 4.5 \text{ mV}$, measuring the energy scale of the surface Dirac cone of Bi₂Te₃. Thus, $J_c \sim 19 \text{ mV}$, and this value can be further reduced by the atomic spin-orbit coupling.

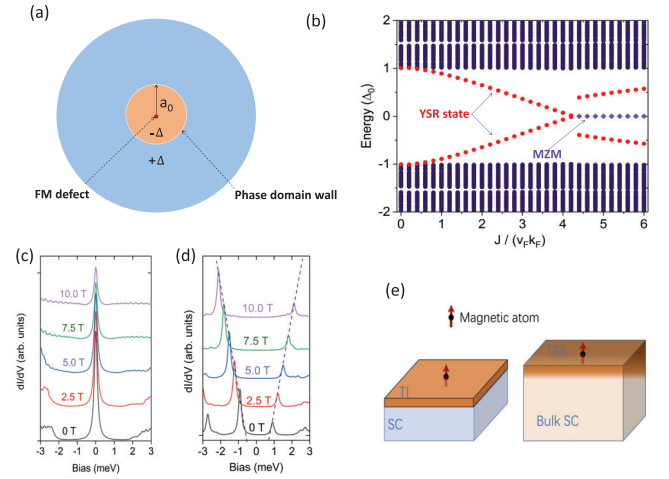


FIG. 3. (a) The $0-\pi$ disk junction. The magnetic defect at center and phase domain wall separating $\pm\Delta$ regimes are marked. a_0 is radius of $-\Delta$ regime and approaches lattice constant. (b) The calculated overall quasiparticle spectrum as change as J under the $0-\pi$ disk junction geometry. The red dots label the YSR states from the magnetic Mn-Bi antisite defect in the center of the disk in (a). The purple diamonds label the MZMs from the phase domain wall shown in (a). The trivial edge modes are not shown (see the SM [35] for details). [(c),(d)] The calculated different response of MZM and YSR state to the external magnetic field, respectively. (e) The proposed two kinds of platforms with magnetic defect to realized MZM. The left one includes topological insulator and superconductor. The right one only is a superconducting topological material.

In addition to impurity-induced trivial YSR states, we now turn to another quasiparticle associated with the zero-energy state. It is important to note that beyond QPT, i.e., $J > J_c$, a phase domain wall emerges for $\Delta(\mathbf{r})$ as shown in Fig. 3(a). This means that $\Delta(\mathbf{r})$ is negative for $r < a_0$ and positive for $r > a_0$, where a_0 is a characteristic length close to the lattice constant of Bi₂Te₃. Consequently, when $J > J_c$, we can further simplify H_{tot} in Eq. (1) to the following form:

$$H_r = H_{\text{sur}} + \Delta_s(\mathbf{r}) \tau_x. \quad (4)$$

Here, $\Delta_s(\mathbf{r}) = -\Delta_1$ for $r < a_0$ and $\Delta_s(\mathbf{r}) = \Delta_2$ for $r > a_0$ with $\Delta_{1/2} > 0$ and $0 < \Delta_1 < \Delta_2$. The phase of $\Delta_{1/2}$ is uniform and is omitted. In the continuum limit, the eigenequation of H_r is

$$H_r(\mathbf{k} \rightarrow -i\nabla)\psi(r, \theta) = E\psi(r, \theta), \quad (5)$$

which can be solved under the boundary conditions of a $0-\pi$ disk junction geometry as illustrated in Fig. 3(a). The $0-\pi$ disk junction is obtained by bending a $0-\pi$ line junction, which introduces a phase factor $e^{i\kappa_0 \tau_0 \sigma_z \theta/2}$ to the wave function $\psi(r, \theta)$ [71]. Thus, the wave function $\psi(r, \theta)$ must satisfy the antiperiodic boundary condition $\psi(r, \theta + 2\pi) = -\psi(r, \theta)$ [60, 71, 72]. We have numerically verified this boundary condition [60]. The details of solving Eq. (5) are provided in the SM [35]. Neglecting the second order terms of k in H_{sur} of Eq. (2), we obtain a pair of MZMs. The wave function of the first MZM takes the form $\psi_1(r, \theta) = [e^{-i\theta/2} u_\uparrow(r), e^{i\theta/2} u_\downarrow(r), e^{-i\theta/2} v_\downarrow(r), -e^{i\theta/2} v_\uparrow(r), 0, 0, 0]^T$, where $u_\sigma(r) = -v_\sigma(r)$, $u_\sigma(r) = a_\sigma J_{\mp 1/2}(k_F r) e^{r/\xi_1}$ for $r < a_0$,

and $u_\sigma(r) = b_\sigma J_{\mp 1/2}(k_F r) e^{-r/\xi_2}$ for $r > a_0$. Here, $J_{\mp 1/2}(k_F r)$ denotes the Bessel functions with $\mp 1/2$ corresponding to spin up and down, respectively. The Fermi wave vector is given by $k_F = \sqrt{\mu^2 - \Lambda_0^2}/v_F$, and the decay length $\xi_{1/2} = v_F/\Delta_{1/2}$. The wave function of the second MZM is $\psi_2(r, \theta) = \mathcal{T}\psi_1(r, \theta)$ where $\mathcal{T} = i\kappa_x\sigma_y\tau_0\mathcal{K}$ represents the emergent time-reversal symmetry operator. When the second order terms of k in H_{sur} of Eq. (2) are considered, the unchanged in-plane spin texture of the surface state still gives rise to effective topological superconductivity [73], leading to the presence of a robust pair of MZMs. In this case, analytical solutions are not available, but numerical calculations yield clear solutions for the MZMs, as demonstrated in Fig. 3(b) (see the SM [35] for details).

In the superconducting state of the 1-UC MnTe/Bi₂Te₃/Fe(Te, Se) system, two types of quasiparticles coexist, as depicted in Fig. 3(b). The first type is the trivial YSR state originating from the magnetic Mn-Bi antisite defect itself. The second type is the MZM bound by the superconducting phase domain wall induced by the defect. These two types of quasiparticles exhibit distinct responses to external magnetic fields and temperature, etc. However, the coexistence and mutual interaction of these quasiparticles can explain all the observed phenomena. First, let's consider the application of an external magnetic field. The energy levels of the YSR states must shift due to the Zeeman coupling, as shown in Fig. 3(d). This behavior has been experimentally observed for the non-zero-energy bound states. On the other hand, a pair of MZMs remains unsplit under an out-of-plane magnetic field. The corresponding wave function forms of the MZM solutions in Eq. (5) remain unchanged, except that k_F is renormalized to $\sqrt{\mu^2 - (\Lambda_0 \pm \mu_B B_z)^2}$, where μ_B represents the Bohr magneton and B_z is the strength of the magnetic field along the z direction. Our calculations indicate that $\mu \sim 100$ meV and $\Lambda_0 \sim 45$ meV ~ 375 T. The experimental magnetic field applied, which is less than 10 T, has a negligible effect on the MZMs. Consequently, the pair of MZMs remains robust against out-of-plane magnetic fields, as illustrated in Fig. 3(c). This robustness is protected by a hidden mirror symmetry, denoted as $\mathcal{M} = i\kappa_x\sigma_y\tau_y$, with a mirror plane along the phase domain wall. However, an in-plane magnetic field in the y direction can break the mirror symmetry and split the pair of MZMs. We suggest further experiments to verify this prediction. Another issue of interest is the effect of temperature. The zero-energy state can only be observed below a temperature significantly lower than T_c . This behavior can also be understood through our self-consistent calculations, which reveal that the quantum phase transition (QPT) is quenched at a much lower temperature than T_c (see the SM [35] for details). The third interesting property relates to the behavior of tunneling spectra under different tunneling transmissions achieved by tuning the tunneling barrier. In experiments conducted on trilayer heterostructures, a saturated value of 0.22 in units of $2e^2/h$ is much smaller than the case of vortices where a value close to saturation at 1 in units of $2e^2/h$. The smaller value of 0.22 strongly indicates that the observed zero-energy state in the trilayer heterostructure experiment originates from the topmost sublayer of the 1-UC Bi₂Te₃ as we propose, and the MnTe

layer inevitably reduces the tunneling transmission. In other words, the MZMs remain hidden, as we have previously pointed out.

Based on our understanding of the underlying physics behind the zero-energy states, we propose improvements and new heterostructures to realize the MZMs, as depicted in Fig. 3(e). In the left plot of Fig. 3(e), the MnTe layer is not necessary, and the substrate Fe(Te, Se) can be replaced by another superconductor such as NbSe₂. The only crucial aspect is to introduce a magnetic impurity or defect on the topmost layer of the Bi₂Te₃ thin film. The advantage of the heterostructure shown in Fig. 3(e) is that the coupling between the magnetic impurity or defect and the top surface of the Bi₂Te₃ thin film can be finely tuned. This tunability provides a method for manipulating the MZMs. Furthermore, the heterostructure can be further simplified by utilizing a single superconducting topological material to replace the Bi₂Te₃/superconductor heterostructure, as demonstrated in the right plot of Fig. 3(e).

There are different scenarios that can be considered to explain the generation of zero-energy states. The first scenario is the spontaneous vortex state. In this case, the MZMs can be regarded as the end states of a one-dimensional vortex line. When the line is very short, as in the case of a thin film, the two end states can couple and split [74]. However, in our system, the pair of MZMs is located in the phase domain wall around the defect in the topmost sublayer of the 1-UC Bi₂Te₃. Therefore, there is no such coupling, and the MZMs remain robust. The second scenario is the possibility of a magnetic skyrmion. In this case, theoretical studies have shown that only skyrmions with a topological charge of $Q = 2$ can bind an MZM [75–77]. However, typically, $Q = 2$ skyrmions are not stable and tend to split into two $Q = 1$ skyrmions. DFT calculations give the AFM-type not FM-type exchange coupling, indicating an AFM exchange coupling rather than the required FM exchange coupling to form conventional skyrmions. Moreover, the size, shape, and density of skyrmions are sensitive to changes in the external magnetic field [78–81]. Therefore, the skyrmion scenario is not preferred in our case. The third scenario is associated with the odd-frequency spin triplet pairing correlation. This correlation is typically observed in complex superconducting and ferromagnetic multi layers [82,83]. In these systems, certain zero energy states can emerge at the interface between the superconducting and ferromagnetic layers. These zero energy states exhibit intriguing characteristics, including their extension lying in the interface, their immunity to external magnetic fields in any direction, and their spin polarization [29,84–86]. These features distinguish them from the MZMs, which are highly localized, robust only against external magnetic fields perpendicular to the plane, and do not exhibit overall spin polarization. These distinctions can be easily identified through experiments.

In summary, we have uncovered the underlying physics behind the robustness of the zero-energy state in the trilayer heterostructure MnTe/Bi₂Te₃/Fe(Te, Se), and find that there are two types of quasiparticles: the YSR state arising from the magnetic Mn-Bi antisite defect itself, and the MZM emerging from the superconducting phase domain induced by the defect. By considering both types of quasi-particles, we are able to explain all the experimental observations.

Moreover, we have proposed simpler platforms that possess advantages for generating and finely tuning MZMs. Our studies provide new strategies for exploring Majorana physics and open up avenues for further investigations in this field.

The authors thank J. P. Hu, D. L. Feng, T. Zhang, Z. Fang, C. Fang, P. Zhang, X. X. Wu, S. B. Zhang, S. S. Qin, F. W. Zheng, H. F. Du, L. Shan, Z. Y. Wang, S. C. Yan, and X. Y. Hou for helpful discussions. This work was financially

supported by the National Key R&D Program of China (Grants No. 2022YFA1403200 and No. 2017YFA0303201), the National Natural Science Foundation of China (Grants No. 92265104, No. 12022413, and No. 11674331), the “Strategic Priority Research Program (B)” of the Chinese Academy of Sciences Grant No. XDB33030100, and the Major Basic Program of Natural Science Foundation of Shandong Province (Grant No. ZR2021ZD01). A portion of this work was supported by the High Magnetic Field Laboratory of Anhui Province, China.

-
- [1] Q. Y. Wang, Z. Li, W. H. Zhang, Z. C. Zhang, J. S. Zhang, W. Li, H. Ding, Y. B. Ou, P. Deng, K. Chang, J. Wen, C. L. Song, K. He, J. F. Jia, S. H. Ji, Y. Y. Wang, L. L. Wang, X. Chen, X. C. Ma, and Q. K. Xue, Interface induced high temperature superconductivity in single unit-cell FeSe Films on SrTiO₃, *Chin. Phys. Lett.* **29**, 037402 (2012).
- [2] S. Y. Tan, Y. Zhang, M. Xia, Z. R. Ye, F. Chen, X. Xie, R. Peng, D. F. Xu, Q. Fan, H. C. Xu, J. Jiang, T. Zhang, X. C. Lai, T. Xiang, J. P. Hu, B. P. Xie, and D. L. Feng, Interface-induced superconductivity and strain-dependent spin density waves in FeSe/SrTiO₃ thin films, *Nat. Mater.* **12**, 634 (2013).
- [3] J. J. Lee, F. T. Schmitt, R. G. Moore, S. Johnston, Y.-T. Cui, W. Li, M. Yi, Z. K. Liu, M. Hashimoto, Y. Zhang, D. H. Lu, T. P. Devereaux, D.-H. Lee, and Z.-X. Shen, Interfacial mode coupling as the origin of the enhancement of T_c in FeSe films on SrTiO₃, *Nature (London)* **515**, 245 (2014).
- [4] N. Hao and J. Hu, Topological Phases in the Single-Layer FeSe, *Phys. Rev. X* **4**, 031053 (2014).
- [5] N. Hao and J. Hu, Topological quantum states of matter in iron-based superconductors: from concept to material realization, *Natl. Sci. Rev.* **6**, 213 (2019).
- [6] Q. Wang, R. Song, and N. Hao, Spin-dependent high-order topological states and corner modes in a monolayer FeSe/GdClO heterostructure, *Phys. Rev. B* **107**, 235406 (2023).
- [7] Z. F. Wang, H. Zhang, D. Liu, C. Liu, C. Tang, C. Song, Y. Zhong, J. Peng, F. Li, C. Nie, L. Wang, X. Zhou, X. Ma, Q. Xue, and F. Liu, Topological edge states in a high-temperature superconductor FeSe/SrTiO₃(001) film, *Nat. Mater.* **15**, 968 (2016).
- [8] J. Shiogai, Y. Ito, T. Mitsuhashi, T. Nojima, and A. Tsukazaki, Electric-field-induced superconductivity in electrochemically etched ultrathin FeSe films on SrTiO₃ and MgO, *Nat. Phys.* **12**, 42 (2016).
- [9] C. Liu, H. Shin, A. Doll, H. Kung, R. P. Day, B. A. Davidson, J. Dreiser, G. Levy, A. Damascelli, C. Piamonteze, and K. Zou, High-temperature superconductivity and its robustness against magnetic polarization in monolayer FeSe on EuTiO₃, *npj Quantum Mater.* **6**, 85 (2021).
- [10] L. R. Tagirov, Low-Field Superconducting Spin Switch Based on a Superconductor/Ferromagnet Multilayer, *Phys. Rev. Lett.* **83**, 2058 (1999).
- [11] V. T. Petrashov, I. A. Sosnin, I. Cox, A. Parsons, and C. Troadec, Giant Mutual Proximity Effects in Ferromagnetic/Superconducting Nanostructures, *Phys. Rev. Lett.* **83**, 3281 (1999).
- [12] R. S. Keizer, S. Goennenwein, T. Klapwijk, G. Miao, G. Xiao, and A. Gupta, A spin triplet supercurrent through the half-metallic ferromagnet CrO₂, *Nature (London)* **439**, 825 (2006).
- [13] P. V. Leksin, N. N. Garif'yanov, I. A. Garifullin, Ya. V. Fominov, J. Schumann, Y. Krupskaya, V. Kataev, O. G. Schmidt, and B. Büchner, Evidence for Triplet Superconductivity in a Superconductor-Ferromagnet Spin Valve, *Phys. Rev. Lett.* **109**, 057005 (2012).
- [14] K. Halterman and O. T. Valls, Emergence of triplet correlations in superconductor/half-metallic nanojunctions with spin-active interfaces, *Phys. Rev. B* **80**, 104502 (2009).
- [15] J. Zhu, I. N. Krivorotov, K. Halterman, and O. T. Valls, Angular Dependence of the Superconducting Transition Temperature in Ferromagnet-Superconductor-Ferromagnet Trilayers, *Phys. Rev. Lett.* **105**, 207002 (2010).
- [16] K. Halterman, O. T. Valls, and M. Alidoust, Spin-Controlled Superconductivity and Tunable Triplet Correlations in Graphene Nanostructures, *Phys. Rev. Lett.* **111**, 046602 (2013).
- [17] Y. N. Khaydukov, G. A. Ovsyannikov, A. E. Sheyerman, K. Y. Constantinian, L. Mustafa, T. Keller, M. A. Uribe-Laverde, Yu. V. Kisilinskii, A. V. Shadrin, A. Kalaboukhov, B. Keimer, and D. Winkler, Evidence for spin-triplet superconducting correlations in metal-oxide heterostructures with noncollinear magnetization, *Phys. Rev. B* **90**, 035130 (2014).
- [18] Y. Saito, Y. Nakamura, M. S. Bahramy, Y. Kohama, J. Ye, Y. Kasahara, Y. Nakagawa, M. Onga, M. Tokunaga, T. Nojima, Y. Yanase, and Y. Iwasa, Superconductivity protected by spin-valley locking in ion-gated MoS₂, *Nat. Phys.* **12**, 144 (2016).
- [19] G. Tkachov, Magnetoelectric Andreev Effect due to Proximity-Induced Nonunitary Triplet Superconductivity in Helical Metals, *Phys. Rev. Lett.* **118**, 016802 (2017).
- [20] A. Srivastava, L. O. Olthof, A. Bernardo, S. Komori, M. Amado, C. Palomares-Garcia, M. Alidoust, K. Halterman, M. Blamire, and J. Robinson, Magnetization Control and Transfer of Spin-Polarized Cooper Pairs into a Half-Metal Manganite, *Phys. Rev. Appl.* **8**, 044008 (2017).
- [21] Z. Tao, F. Chen, L. Zhou, B. Li, Y. Tao, and J. Wang, Superconductivity switch from spin-singlet to -triplet pairing in a topological superconducting junction, *J. Phys.: Condens. Matter* **30**, 225302 (2018).
- [22] P. Niu, L. Liu, X. Su, L. Dong, Y. Shi, and H.-G. Luo, Spin-resolved transport physics induced by a Majorana-fermion zero mode, *AIP Adv.* **9**, 125115 (2019).
- [23] Y. V. Fominov, A. A. Golubov, T. Y. Karminskaya, M. Y. Kupriyanov, R. G. Deminov, and L. R. Tagirov, Superconducting triplet spin valve, *JETP Lett.* **91**, 308 (2010).

- [24] Y. V. Fominov, A. A. Golubov, and M. Y. Kupriyanov, Triplet proximity effect in FSF trilayers, *JETP Lett.* **77**, 510 (2003).
- [25] K. Halterman, P. H. Barsic, and O. T. Valls, Odd Triplet Pairing in Clean Superconductor/Ferromagnet Heterostructures, *Phys. Rev. Lett.* **99**, 127002 (2007).
- [26] A. A. Jara, C. Safranski, I. N. Krivorotov, C.-T. Wu, A. N. Malmi-Kakkada, O. T. Valls, and K. Halterman, Angular dependence of superconductivity in superconductor/spin-valve heterostructures, *Phys. Rev. B* **89**, 184502 (2014).
- [27] K. Halterman, O. T. Valls, and P. H. Barsic, Induced triplet pairing in clean *s*-wave superconductor/ferromagnet layered structures, *Phys. Rev. B* **77**, 174511 (2008).
- [28] K. Halterman and M. Alidoust, Half-metallic superconducting triplet spin valve, *Phys. Rev. B* **94**, 064503 (2016).
- [29] M. Alidoust, K. Halterman, and O. T. Valls, Zero-energy peak and triplet correlations in nanoscale superconductor/ferromagnet/ferromagnet spin valves, *Phys. Rev. B* **92**, 014508 (2015).
- [30] S. Ding, C. Chen, Z. Cao, D. Wang, Y. Pan, R. Tao, D. Zhao, Y. Hu, T. Jiang, Y. Yan, Z. Shi, X. Wan, D. Feng, and T. Zhang, Observation of robust zero-energy state and enhanced superconducting gap in a trilayer heterostructure of MnTe/Bi₂Te₃/Fe(Te, Se), *Sci. Adv.* **8**, eabq4578 (2022).
- [31] Y. Zhang, J. Huang, C. Zhang, P. Wang, Z. Wang, T. Wang, Z. Xing, and D. Y. Xing, Proximity-effect-induced superconductivity in Bi₂Te₃/FeSe_{0.5}Te_{0.5} thin-film heterostructures with different interface conditions, *Phys. Rev. B* **102**, 064503 (2020).
- [32] H. Zhao, B. Rachmilowitz, Z. Ren, R. Han, J. Schneeloch, R. Zhong, G. Gu, Z. Wang, and I. Zeljkovic, Superconducting proximity effect in a topological insulator using Fe(Te, Se), *Phys. Rev. B* **97**, 224504 (2018).
- [33] S. Li, J. Wu, B. Liang, L. Liu, W. Zhang, N. Wazir, J. Zhou, Y. Liu, Y. Nie, Y. Hao, P. Wang, L. Wang, Y. Shi, and S. Li, Antiferromagnetic α -MnTe: Molten-salt-assisted chemical vapor deposition growth and magneto-transport properties, *Chem. Mater.* **34**, 873 (2022).
- [34] D. Kriegner, K. Výborný, K. Olejník, H. Reichlová, V. Novák, X. Martí, J. Gazquez, V. Saidl, P. Němec, V. V. Volobuev, G. Springholz, V. Holý, and T. Jungwirth, Multiple-stable anisotropic magnetoresistance memory in antiferromagnetic MnTe, *Nat. Commun.* **7**, 11623 (2016).
- [35] See Supplemental Material at <http://link.aps.org/supplemental/10.1103/PhysRevB.108.L100509> for details about the DFT calculations, the self-consistent solutions of the BdG equations in lattice model, the proof for the quivalence between vortex case and impurity case, and the solutions for the Majorana zero modes. which contains Refs. [36–42].
- [36] G. Kresse and J. Furthmüller, Efficient iterative schemes for *ab initio* total-energy calculations using a plane-wave basis set, *Phys. Rev. B* **54**, 11169 (1996).
- [37] G. Kresse and D. Joubert, From ultrasoft pseudopotentials to the projector augmented-wave method, *Phys. Rev. B* **59**, 1758 (1999).
- [38] P. E. Blöchl, Projector augmented-wave method, *Phys. Rev. B* **50**, 17953 (1994).
- [39] J. P. Perdew, K. Burke, and M. Ernzerhof, Generalized Gradient Approximation Made Simple, *Phys. Rev. Lett.* **77**, 3865 (1996).
- [40] H.-Z. Lu, W.-Yu. Shan, W. Yao, Q. Niu, and S.-Q. Shen, Massive Dirac fermions and spin physics in an ultrathin film of topological insulator, *Phys. Rev. B* **81**, 115407 (2010).
- [41] A. H. Castro Neto, F. Guinea, N. M. R. Peres, K. S. Novoselov, and A. K. Geim, The electronic properties of graphene, *Rev. Mod. Phys.* **81**, 109 (2009).
- [42] X. Wu, S. B. Chung, C. Liu, and E.-A. Kim, Topological orders competing for the Dirac surface state in FeSeTe surfaces, *Phys. Rev. Res.* **3**, 013066 (2021).
- [43] F. Ma, W. Ji, J. Hu, Z.-Y. Lu, and T. Xiang, First-Principles Calculations of the Electronic Structure of Tetragonal α -FeTe and α -FeSe Crystals: Evidence for a Bicollinear Antiferromagnetic Order, *Phys. Rev. Lett.* **102**, 177003 (2009).
- [44] W. Li, S. Dong, C. Fang, and J. Hu, Block antiferromagnetism and checkerboard charge ordering in the alkali-doped iron selenides R_{1-x}Fe_{2-y}Se₂, *Phys. Rev. B* **85**, 100407(R) (2012).
- [45] H.-Y. Cao, S. Chen, H. Xiang, and X.-G. Gong, Antiferromagnetic ground state with pair-checkerboard order in FeSe, *Phys. Rev. B* **91**, 020504(R) (2015).
- [46] F. Zheng, L.-L. Wang, Q.-K. Xue, and P. Zhang, Band structure and charge doping effects of the potassium-adsorbed FeSe/SrTiO₃ system, *Phys. Rev. B* **93**, 075428 (2016).
- [47] Q. Wang, Y. Shen, B. Pan, X. Zhang, K. Ikeuchi, K. Iida, A. D. Christianson, H. C. Walker, D. T. Adroja, M. Abdel-Hafiez, X. Chen, D. A. Chareev, A. N. Vasiliev, and J. Zhao, Magnetic ground state of FeSe, *Nat. Commun.* **7**, 12182 (2016).
- [48] P. C. Dai, Antiferromagnetic order and spin dynamics in iron-based superconductors, *Rev. Mod. Phys.* **87**, 855 (2015).
- [49] S.-C. Li, Y. Gan, J.-H. Wang, K.-J. Ran, and J.-S. Wen, Magnetic neutron scattering studies on the Fe-based superconductor system Fe_{1+y}Te_{1-x}Se_x, *Acta Phys. Sin.* **64**, 097503 (2015).
- [50] T. M. McQueen, A. J. Williams, P. W. Stephens, J. Tao, Y. Zhu, V. Ksenofontov, F. Casper, C. Felser, and R. J. Cava, Tetragonal-to-Orthorhombic Structural Phase Transition at 90 K in the Superconductor Fe_{1.01}Se, *Phys. Rev. Lett.* **103**, 057002 (2009).
- [51] T. M. McQueen, Q. Huang, V. Ksenofontov, C. Felser, Q. Xu, H. Zandbergen, Y. S. Hor, J. Allred, A. J. Williams, D. Qu, J. Checkelsky, N. P. Ong, and R. J. Cava, Extreme sensitivity of superconductivity to stoichiometry in Fe_{1+ δ} Se, *Phys. Rev. B* **79**, 014522 (2009).
- [52] J. Wen, Magnetic neutron scattering studies on the Fe-based superconductor system Fe_{1+y}Te_{1-x}Se_x, *Ann. Phys.* **358**, 92 (2015).
- [53] D. Nevola, H. X. Li, J.-Q. Yan, R. G. Moore, H.-N. Lee, H. Miao, and P. D. Johnson, Coexistence of Surface Ferromagnetism and a Gapless Topological State in MnBi₂Te₄, *Phys. Rev. Lett.* **125**, 117205 (2020).
- [54] P. Swatek, Y. Wu, L.-L. Wang, K. Lee, B. Schruink, J. Yan, and A. Kaminski, Gapless Dirac surface states in the antiferromagnetic topological insulator MnBi₂Te₄, *Phys. Rev. B* **101**, 161109(R) (2020).
- [55] Y.-J. Hao, P. Liu, Y. Feng, X.-M. Ma, E. F. Schwier, M. Arita, S. Kumar, C. Hu, R. Lu, M. Zeng, Y. Wang, Z. Hao, H.-Y. Sun, K. Zhang, J. Mei, N. Ni, L. Wu, K. Shimada, C. Chen, Q. Liu *et al.*, Gapless Surface Dirac Cone in Antiferromagnetic Topological Insulator MnBi₂Te₄, *Phys. Rev. X* **9**, 041038 (2019).
- [56] Y. Hu, L. Xu, M. Shi, A. Luo, S. Peng, Z. Y. Wang, J. J. Ying, T. Wu, Z. K. Liu, C. F. Zhang, Y. L. Chen, G. Xu, X.-H. Chen, and J.-F. He, Universal gapless Dirac cone and tunable topological states in (MnBi₂Te₄)_m(Bi₂Te₄)_n, *Phys. Rev. B* **101**, 161113(R) (2020).

- [57] N. D. Mermin and H. Wagner, Absence of Ferromagnetism or Antiferromagnetism in One- or Two-Dimensional Isotropic Heisenberg Models, *Phys. Rev. Lett.* **17**, 1133 (1966).
- [58] G. Qian, M. Shi, H. Chen, S. Zhu, J. Hu, Z. Huang, Y. Huang, X. H. Chen, and H. J. Gao, Spin-flop transition and Zeeman effect of defect-localized bound states in the antiferromagnetic topological insulator MnBi_2Te_4 , *Nano Res.* **16**, 1101 (2023).
- [59] H.-Z. Lu, A. Zhao, and S.-Q. Shen, Quantum Transport in Magnetic Topological Insulator Thin Films, *Phys. Rev. Lett.* **111**, 146802 (2013).
- [60] R. Song, P. Zhang, X.-T. He, and N. Hao, Ferromagnetic impurity induced Majorana zero mode in iron-based superconductors, *Phys. Rev. B* **106**, L180504 (2022).
- [61] A. V. Balatsky, I. Vekhter, and J.-X. Zhu, Impurity-induced states in conventional and unconventional superconductors, *Rev. Mod. Phys.* **78**, 373 (2006).
- [62] M. E. Flatté and J. M. Byers, Local Electronic Structure of a Single Magnetic Impurity in a Superconductor, *Phys. Rev. Lett.* **78**, 3761 (1997).
- [63] R. Kümmel, Electronic structure of superconductors with dilute magnetic impurities, *Phys. Rev. B* **6**, 2617 (1972).
- [64] A. Yazdani, B. A. Jones, C. P. Lutz, M. F. Crommie, and D. M. Eigler, Probing the local effects of magnetic impurities on superconductivity, *Science* **275**, 1767 (1997).
- [65] M. I. Salkola, A. V. Balatsky, and J. R. Schrieffer, Spectral properties of quasiparticle excitations induced by magnetic moments in superconductors, *Phys. Rev. B* **55**, 12648 (1997).
- [66] T. Meng, J. Klinovaja, S. Hoffman, P. Simon, and D. Loss, Superconducting gap renormalization around two magnetic impurities: From Shiba to Andreev bound states, *Phys. Rev. B* **92**, 064503 (2015).
- [67] S.-I. Suzuki, T. Sato, and Y. Asano, Odd-frequency Cooper pair around a magnetic impurity, *Phys. Rev. B* **106**, 104518 (2022).
- [68] Y. Luh, Bound state in superconductors with paramagnetic impurities, *Acta Phys. Sin.* **21**, 75 (1965).
- [69] H. Shiba, Classical spins in superconductors, *Prog. Theor. Phys.* **40**, 435 (1968).
- [70] A. I. Rusinov, Theory of gapless superconductivity in alloys containing paramagnetic impurities, *Sov. Phys. JETP* **29**, 1101 (1969).
- [71] L. Fu and C. L. Kane, Superconducting Proximity Effect and Majorana Fermions at the Surface of a Topological Insulator, *Phys. Rev. Lett.* **100**, 096407 (2008).
- [72] R. Song, P. Zhang, and N. Hao, Phase-Manipulation-Induced Majorana Mode and Braiding Realization in Iron-Based Superconductor $\text{Fe}(\text{Te}, \text{Se})$, *Phys. Rev. Lett.* **128**, 016402 (2022).
- [73] S. Y. Xu, N. Alidoust, I. Belopolski, A. Richardella, C. Liu, M. Neupane, G. Bian, S.-H. Huang, R. Sankar, C. Fang, B. Dellabetta, W. Dai, Q. Li, M. J. Gilbert, F. Chou, N. Samarth, and M. Z. Hasan, Momentum-space imaging of Cooper pairing in a half-Dirac-gas topological superconductor, *Nat. Phys.* **10**, 943 (2014).
- [74] B. Fu and S.-Q. Shen, Anomalous coherence length of majorana zero modes at vortices in superconducting topological insulators, *Phys. Rev. B* **107**, 184517 (2023).
- [75] G. Yang, P. Stano, J. Klinovaja, and D. Loss, Majorana bound states in magnetic skyrmions, *Phys. Rev. B* **93**, 224505 (2016).
- [76] U. Güngördü, S. Sandhoefner, and A. A. Kovalev, Stabilization and control of Majorana bound states with elongated skyrmions, *Phys. Rev. B* **97**, 115136 (2018).
- [77] S. Rex, I. V. Gornyi, and A. D. Mirlin, Majorana bound states in magnetic skyrmions imposed onto a superconductor, *Phys. Rev. B* **100**, 064504 (2019).
- [78] M. C. Langner, S. Roy, S. K. Mishra, J. C. T. Lee, X. W. Shi, M. A. Hossain, Y. D. Chuang, S. Seki, Y. Tokura, S. D. Kevan, and R. W. Schoenlein, Coupled Skyrmion Sublattices in Cu_2OSeO_3 , *Phys. Rev. Lett.* **112**, 167202 (2014).
- [79] R. Ozawa, S. Hayami, and Y. Motome, Zero-Field Skyrmions with a High Topological Number in Itinerant Magnets, *Phys. Rev. Lett.* **118**, 147205 (2017).
- [80] F. Rendell-Bhatti, R. J. Lamb, J. W. van der Jagt, G. W. Paterson, H. J. M. Swagten, and D. McGruther, Spontaneous creation and annihilation dynamics and strain-limited stability of magnetic skyrmions, *Nat. Commun.* **11**, 3536 (2020).
- [81] S. L. Zhang, W. W. Wang, D. M. Burn, H. Peng, H. Berger, A. Bauer, C. Pfeleiderer, G. van der Laan, and T. Hesjedal, Manipulation of skyrmion motion by magnetic field gradients, *Nat. Commun.* **9**, 2115 (2018).
- [82] R. Beiranvand, H. Hamzehpour, and M. Alidoust, Tunable anomalous Andreev reflection and triplet pairings in spin-orbit-coupled graphene, *Phys. Rev. B* **94**, 125415 (2016).
- [83] R. Beiranvand, H. Hamzehpour, and M. Alidoust, Nonlocal Andreev entanglements and triplet correlations in graphene with spin-orbit coupling, *Phys. Rev. B* **96**, 161403(R) (2017).
- [84] M. Alidoust and K. Halterman, Half-metallic superconducting triplet spin multivalves, *Phys. Rev. B* **97**, 064517 (2018).
- [85] K. Halterman and M. Alidoust, Induced energy gap in finite-sized superconductor/ferromagnet hybrids, *Phys. Rev. B* **98**, 134510 (2018).
- [86] K. Halterman, M. Alidoust, R. Smith, and S. Starr, Supercurrent diode effect, spin torques, and robust zero-energy peak in planar half-metallic trilayers, *Phys. Rev. B* **105**, 104508 (2022).